Desalination and Water Treatment
www.deswater.com
doi: 10.1080/19443994.2013.795020

51 (2013) 3988–3994
May

Taylor & Francis
Taylor & Francis Group

Carbon nanotube and carbon nanofiber composite films grown on different graphite substrate for capacitive deionization

Yong Liu, Haibo Li, Chunyang Nie, Likun Pan*, Zhuo Sun

Engineering Research Center for Nanophotonics and Advanced Instruments, Ministry of Education, Department of Physics, East China Normal University, Shanghai 200062, China
Tel. +86 21 62234132; Fax: +86 21 62234321; email: lkpan@phy.ecnu.edu.cn

Received 3 May 2012; Accepted 19 March 2013

ABSTRACT

The carbon nanotube and carbon nanofibre (CNT–CNF) composite films are synthesized on different graphite substrate by low-pressure and low-temperature chemical vapor deposition. Scanning electron microscopy measurement and N_2 adsorption experiment show that CNT–CNF composite films have network structure with optimal pore size distribution, which is beneficial to capacitive deionization. Atomic force microscopy result indicates that there is a strong correlation between the surface roughness of graphite and their thickness. Furthermore, the electrosorptive performance in salt solutions by employing as-grown CNT–CNF composite film is studied and found that the properties of the graphite substrate play a vital role in electrosorptive performance of CNT–CNF composite films by influencing their network structures.

Keywords: Chemical vapor deposition; Carbon nanotube and carbon nanofiber; Capacitive deionization

1. Introduction

Since the discovery by Iijima in 1991 [1], carbon nanotube (CNT) has continued to arouse great excitement among the scientific community in light of their promise to exhibit exceptional properties, such as high specific surface area, low density, high specific capacitance, excellent electrical conductivity, and high chemical stability, which makes them as promising candidate in the application of electrochemical double layer capacitors [2], fuel cells [3], and capacitive deionization (CDI) [4–6]. Recent developments in chemical vapor deposition (CVD) have made it possible to grow a massive quantity of CNT in a low cost and controlled manner by optimizing metal catalysts [7], flow rate [8], substrates [9], carrier gas [10], etc. Concerning the substrates as catalyst support, it was found that its quality is of considerable importance. Research have been carried out to explore the effect of substrate such as porous silicon [11], transitional metal-base alloy [12], and glass substrate [13] on the growth of CNT because the surface and structure of substrate can affect the activity of catalyst and accessibility of gas molecules to the catalyst. Fan et al. [11] who had synthesized massive arrays of monodi-

*Corresponding author.

Presented at the 2012 Qingdao International Desalination Conference June 26–29, 2012, Qingdao, China

spersed CNT that were self-oriented on patterned porous silicon and plain silicon substrates, reported that catalytic particle size and growth rate of CNT could be controlled by substrate design. Park et al. [12] had interpreted the effect of experimental conditions on the synthesis of CNT on metallic substrates by a sequential combination of plasma-enhanced CVD and thermal CVD. In their study, synthesized CNT was curly in shape, and showed that proper pretreatment of the substrate surface was beneficial to the growth of CNT with particular morphology that we wanted. Li and Hirose [13] had used Ni-base alloy to fabricate CNT and pointed out that aligned CNT was exclusively synthesized by appropriate treatment of the substrate.

CDI with CNT electrodes is a novel technology for removing ionic species from aqueous solutions. In our previous work [14–16], graphite substrate, due to its optimum conductivity and outstanding chemical stability, was successfully employed to grow CNT–CNF composite film by low-pressure CVD (LPCVD) system for electrosorption of ions from concentrated water. The deionization performance of CNT–CNF as electrosorptive electrode material had been found to depend on the surface morphology and microstructure of CNT–CNF film. The CNT–CNF electrode with suitable pore size distribution would facilitate the fast transfer of salt ions and thereby achieve high electrosorptive capacity. As mentioned above, the substrate largely affects the surface structure of CNT. Thus, it is necessary to further explore the role of substrate played on performance of CNT by influencing its microstructure. In this work, CNT–CNF composite films were grown on different graphite substrates. The pore size distribution, pore structure of CNT–CNF composite films, and their electrosorptive properties were investigated. Furthermore, the possible growth mechanism of CNT–CNF grown on different graphite substrate was also discussed.

2. Experimental

2.1. Preparation of CNT–CNF composite film electrodes

The low-temperature and low-pressure chemical vapor deposition system (Shanghai Nanoking Co. Ltd.), was used to fabricate CNT–CNF composite film electrodes. Acetylene was used as the carbon feedstock and hydrogen as the carrier/dilution gas. The growth pressure was kept 20 kPa. The flow rate of acetylene and hydrogen was fixed at 50 and 100 sccm, respectively. The growth of CNT–CNF was carried out for 30 min at a temperature of 550˚C. Graphite layers with different thickness and resistivity were used as substrates. Each graphite substrate was 70 mm wide × 80 mm long × 0.3 mm thick, and had a flow-through hole with the diameter of 6 mm. About 20 nm of nickel layer as a catalyst was deposited on the graphite layers by magnetic sputtering system (Shanghai Nanoking Co. Ltd.). Then the CNT–CNF composite films were directly grown and firmly anchored on the supporting graphite substrates (current collector). The monolithic forms and simultaneous combination of current collector and CNT–CNF composite films were realized. Good electrical connection to external power supply was ensured. The as-grown CNT–CNF film electrodes were immersed into 1 M HCl solution to get rid of nickel catalyst to avoid the influence of nickel during the electrosorption.

2.2. Characterization of CNT–CNF composite films

The surface morphology and structure of CNT–CNF composite films were examined by scanning electron microscopy (SEM, JEOL JSM-LV5610), transmission electron microscope (TEM, JEOL-2010) and Raman spectroscopy (Renishaw inVia), respectively. The X-ray diffraction (XRD) pattern was performed on a Figaku (Japan) D/max-γ A X-ray diffractometer with Cu-K radiation ($\lambda = 1.54178$ Å). The pore size distribution and Brunauer–Emmett–Teller (BET) specific surface area of the CNT–CNF composite films were deduced from the N2 physical adsorption measurement data which were obtained with (ASAP 2010) Accelerated Surface Area and Porosimetry System (Micrometitics, Norcross, GA). The surface roughness of various graphite substrates without any disposal was investigated by atomic force microscopy (AFM) in contact mode. Electrochemical measurements of CNT–CNF film were also examined by the electrochemical workstation (CHI 660 A, Covarda) in a three-compartment cell at ambient temperature. CNT–CNF film electrodes, platinum plate, and saturated calomel electrode were used as the working electrode, the counter electrode, and the reference electrode, respectively. The potential sweep cyclic voltammetry (CV) measurement was carried out in the 1 mol/l KCl solution.

2.3. Graphite layer

Several graphite layers (Qingdao Rockwell Advanced Materials Co. Ltd, Qingdao China) were used as the growing substrate of CNT–CNF. The CNT–CNF composite films grown on different graphite substrates were defined as sample 1, sample 2, sample 3, sample 4, and sample 5, in the consequence of the graphite thickness of 0.3, 0.4, 0.5, 0.7, and

Table 1
The main parameters of graphite substrates

Graphite substrate	Thickness (mm)	Resistivity (Ω/cm)	Rms roughness (nm)
Sample 1	0.3	7×10^{-6}	50.153
Sample 2	0.4	8×10^{-6}	29.581
Sample 3	0.5	7×10^{-6}	17.823
Sample 4	0.7	9×10^{-6}	16.918
Sample 5	1.0	7×10^{-6}	29.190

1.0 mm. The main characteristics of graphite substrate were listed in Table 1. The graphite substrates for sample 2 and 4, with a value of 8×10^{-6} and $9 \times 10^{-6}\,\Omega$/cm, respectively, had larger resistivities than the ones for sample 1, 3, and 5 with a value of $7 \times 10^{-6}\,\Omega$/cm.

2.4. Electrosorptive unit cell setup

The electrosorptive unit cell shown in Fig. 1 was employed. The assembly of one-half of the unit cell is in the order: retaining plate/rubber gasket/electrode/nylon spacer. Retaining plate is made of polymethyl methacrylate plate. The spacing of 1 mm between the electrodes is maintained by rectangular nylon spacer and the rubber spacer.

2.5. Batch-mode electrosorptive experiments

To investigate the electrosorptive capacity of CDI system whose electrode used different as-grown samples, batch-mode experiments were conducted in a continuously recycling system including an electrosorptive unit cell. In each experiment, the solution was continuously pumped from a peristaltic pump into the cell and the effluent returned to the unit cell. The solution volume was maintained at 44 ml and the solution temperature was kept at 298 K. Meanwhile, the amplitude of the applied voltage was 1.2 V at which no electrolysis of water happens. The experiment was performed at the volume flow rate of 40 ml/min in NaCl solution that had an initial conductivity slightly around 50 μS/cm. The relationship between conductivity and concentration was obtained according to a calibration table made prior to the experiment. The concentration variation of NaCl solution was continuously monitored and measured at the outlet of the unit cell by using an ion conductivity meter.

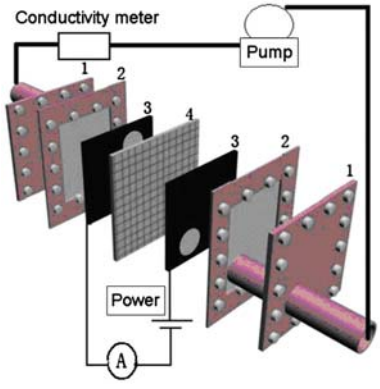

Fig. 1. Schematic of batch-mode experiment and electrosorptive unit cell: (1) retaining plate, (2) rubber gasket, (3) CNT–CNF composite film electrode, and (4) nylon spacer.

In our experiment, the salt removal is defined as follows:

$$\text{Salt removal}\,(\%) = \frac{\phi - \phi_0}{\phi} \times 100 \quad (1)$$

where ϕ is initial conductivity and ϕ_0 is the final conductivity.

3. Results and discussion

3.1. Morphology and structure of CNT–CNF composite films

Typical scanning electron microscopy (SEM) and transmission electron microscope (TEM) images of the CNT–CNF composite films are shown in Fig. 2(a-f). As can be seen, CNT–CNF composite films have a randomly oriented morphology and their diameters vary with different substrates. From Fig. 2, the white dots, corresponding to nickel crystalline inclusions, can be observed at the tip of CNT–CNF, which indicates the tip growth mechanism of CNT–CNF in this work. The CNF and CNT are entangled and form a continuous electroconducting network microstructure. Such network structure ensures a low mass transfer and allows hydrated ions easily to enter through the pores of the CNT–CNF film electrodes and to hold on the electrical double layer when a direct electrical voltage is applied on the electrodes, which is ideal for the electrosorption [17].

Fig. 3(a) exhibits the typical Raman spectra of different samples. The two main modes D at 1,350 and G at 1,580 cm^{-1} are observed. Generally, the G peak corresponds to the tangential stretching (E_{2g}) mode of highly oriented pyrolytic graphite, which indicates the presence of crystalline graphitic carbon in the carbon

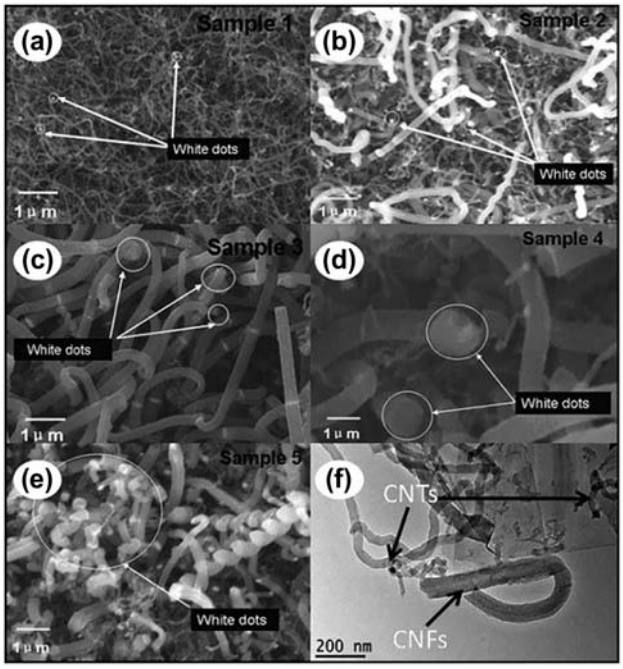

Fig. 2. Typical SEM images of (a) sample 1, (b) sample 2, (c) sample 3, (d) sample 4, (e) sample 5, and (f) TEM image of sample 2.

nanomaterials, while D peak represents the disorder-induced feature due to the finite particle size effect or lattice distortion [18,19]. The ratio of the intensity of D peak to G peak (I_D/I_G) is related to the amount of defects in the carbon products. The I_D/I_G values of different samples are shown in the Fig. 3(b). It is well known that the presence of defects causes an increase in ability for accumulation of charges [20] and the adsorptive capacity for ions [21], which may be beneficial for charge transfer in the electrosorptive process. From Fig. 3(b), it can be observed that sample 1 exhibits the highest ratio of I_D to I_G and thus maybe has an excellent salt removal.

The XRD patterns (not shown here) of all samples show that they have a similar XRD profiles. They reveal three diffraction peaks located at 26.6˚, 44˚, and 56.8˚ which are associated to the (002), (100), and (004) phases, respectively. As illustrated previously [22], they correspond to a typical XRD pattern for CNTs.

3.2. Surface area and pore size distribution analysis

BET surface area and micro- and mesoporous volumes were carried out on a Porosimetry System. The BET equation was used to determine the surface area and the Dubinin–Radushkevich equation was used to deduce micropore. The nitrogen adsorption isotherm and the pore size distribution of CNT–CNF samples

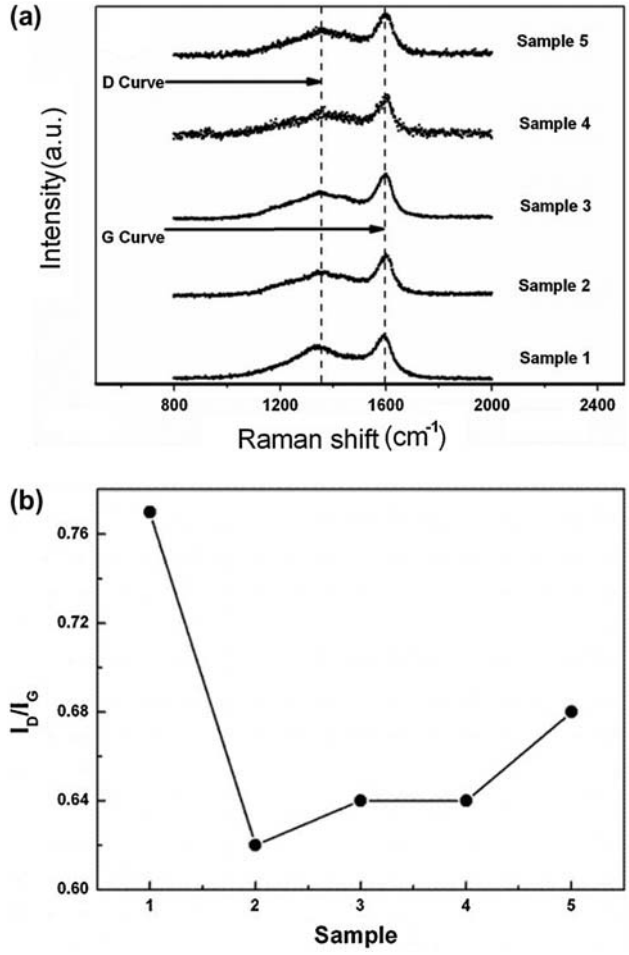

Fig. 3. (a) Raman spectra of different CNT–CNF film samples and (b) The ratio of I_D and I_G derived from Raman spectra.

are shown in Fig. 4. Cryogentic nitrogen isotherm of CNT–CNF composite films exhibits a type IV nitrogen adsorption isotherm, as shown in Fig. 4(a). It can be seen that there is a hysteresis loop typical of a mesoporous material, where desorption required definitively higher energy than adsorption [23]. The initial uptake near 0.01 P_0 (P_0 is the saturation pressure of nitrogen gas at 77 K) indicates the presence of micropores. The gradual increase of the volume adsorbed in the mid-pressure range represents the development of various sizes of mesopores. The adsorption isotherms show no saturation in the large-pressure range, which means wide size distribution in the CNT–CNF composite films. The pore size distribution in Fig. 4(b) shows a majority of pore volume is mainly associated with pores ranging from pore diameter of 2–10 nm corresponding to the range of mesorpores according to the IUPAC classification in which the pore size is divided into three groups: micropores (pore width

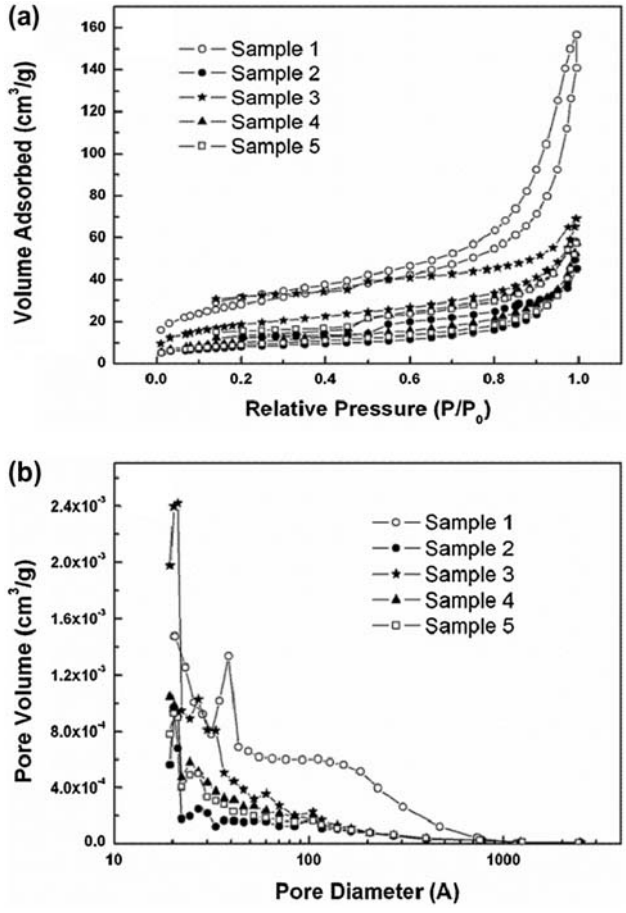

Fig. 4. (a) Nitrogen adsorption isotherms and (b) pore size distribution of different CNT–CNF samples.

<2 nm), mesopores (between 2 and 50 nm), and macropores (>50 nm).

The specific surface area and pore size distribution test results of different samples are listed in Table 2. As known, the pore size distribution of electrodes has a significant influence on electrosorptive capacity. Larger amount of macropores will correspond to lower surface area and lower electrosorptive capacity. On the other hand, micropores (<2 nm) will increase electrical double-layer overlapping effect [24] and reduce electrosorptive capacity [25]. In this work, the proportion of micropore volume in the total pore volume is only about 0.02–1.6% for all the samples and macropores (>50 nm) can be also neglected as indicated in Fig. 4(b). As a result, the pores of CNT–CNF composite films in our experiments are mainly composed of mesopores, which can be confirmed by the average pore diameters of about 6–8 nm as shown in Table 2. Such a pore size distribution is very suitable for the electrosorption. The values of specific surface area and pore volume of all samples, which critically affects the electrosorptive performance, follow the same order: sample 1 > sample 3 > sample 4 > sample 5 > sample 2. The larger specific surface area can accommodate more adsorbed ions, so that sample 1 should be able to deionize with best efficiency.

3.3. Electrochemical characteristics of CNT–CNF films

The specific capacitance, C, is obtained from the CV curve using the equation shown as below:

$$C = \frac{\bar{i}}{sv} \tag{2}$$

where $\bar{i}$, s, and v are average current, surface area of CNT–CNF composite films, and scan rate, respectively. The specific capacitance of CNT–CNF films is shown in Fig. 5. The potential scan rate of each test is set at 50 mV/s with a potential range of −0.5 to 0.5 V. From Fig. 6, it can be seen that the sample 1 has the lowest capacitance among all the samples, with a value of 0.529 F/m^2, while sample 2 and sample 5 nearly have the similar capacitances with a value of 1.517 and 1.455 F/m^2, respectively. Typically, it is believed that the electrochemical characteristics of porous materials have played a significant role in electrosorption and high capacitance is related to high salt removal.

Table 2
Specific surface area, pore volume, and average pore diameter of different CNT–CNF samples

Sample	Total specific surface area (m^2g^{-1})	Micropore specific surface area (m^2g^{-1})	Total pore volume (cm^3g^{-1})	Micropore volume (cm^3g^{-1})	Average pore diameter (nm)
1	102.7	9.3	0.17	0.0028	6.75
2	28.9	3.2	0.05	0.0008	7.42
3	68.6	2.6	0.09	0.0002	4.98
4	38.1	1.9	0.07	0.0001	6.91
5	33.1	1.4	0.06	0.00001	7.59

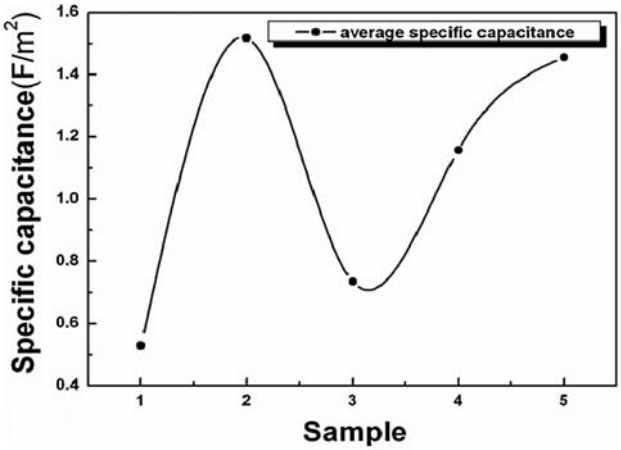

Fig. 5. The specific capacitances of the samples.

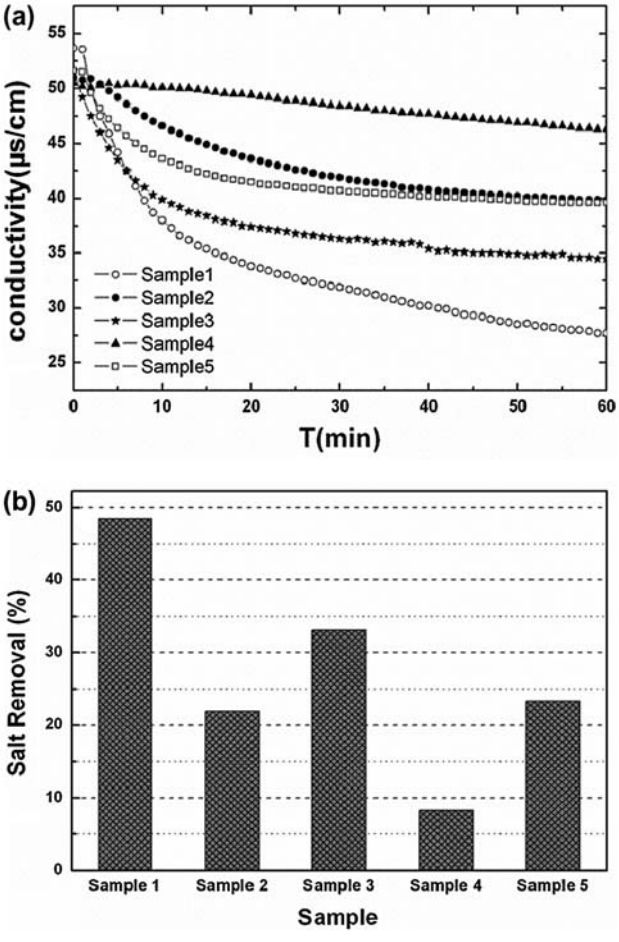

Fig. 6. (a) The conductivity transients in NaCl solution by using different CNT–CNF samples, and (b) the salt removal of different CNT–CNF samples.

3.4. Electrosorptive capacity

Fig. 6(a) shows conductivity transients in NaCl solution for different samples during batch-mode experiments. When the voltage is applied to the CNT–CNF electrodes, the ions are electrosorbed onto the electrode surface and the conductivity is decreased till the electrode is saturated by ions. The charge processes last about 60 min. The salt removal of samples 1–5 is 48.4, 21.9, 33.1, 8.3, and 23.3%, respectively, which follows an order: sample 1 > sample 3 > sample 5 > sample 2 > sample 4, as showed in the Fig. 6(b). Such an order deviates from estimated deionization trend based on the values of specific surface area or pore volume of the samples. Therefore, there surely exist other contributions to deionization performance. It has been mentioned that graphite substrates for sample 1, 3, and 5 have better conduction than the ones for sample 2 and 4. It is well known that the surface resistance of the electrodes consumes the voltage, which causes the actual voltage used on the CDI process are smaller than the applied voltage. Higher resistance of the electrode surface means the higher voltage wasting and the smaller actual voltage, resulting in the lower electrosorptive capacity [14], and therefore the resistivity of substrate should affect electrosorptive performance. As mentioned above, the defects on CNT–CNF surface, indicated by the ratio of I_D to I_G in Raman spectra, will also contribute to the deionization efficiency. Among all the samples, sample 1 displays best electrosorptive capacity due to its larger specific surface area and pore volume, lower resistivity of the substrate, and more surface defects.

The root meaning square (rms) values, obtained by AFM measurement and used to characterize the surface roughness of various graphite, are listed in Table 1. The graphite substrate for sample 1 exhibits highest rms roughness (50.153 nm) while the one for sample 4 has a lowest value (16.918 nm), which can explain why sample 1 and sample 4 have largest and smallest diameters in all samples, as shown in Fig. 1. Although the diameter of CNT is not in direct proportion to its size of pores (including internal and external pores), the smaller diameter, in some degree, can reflect its larger specific surface area. As a result, the morphology and microstructure of CNT–CNF in our experiments is not directly related to the thickness but to the roughness of the graphite substrates. Rougher graphite substrate may facilitate the growth of CNT–CNF composite films with more suitable microstructure for electrosorption.

4. Conclusions

The CNT–CNF composite films were synthesized on different graphite substrates and their electrosorptive performance were consequently investigated. The results showed that the graphite substrate plays an

important role in electrosorptive performance of CNT–CNF composite films by influencing their microstructures. When selecting the graphite substrate for the fabrication of CNT–CNF composite electrode, its surface roughness and resistivity will be two critical factors to be considered in order to obtain the CNT–CNF composite film with better deionization efficiency.

Acknowledgment

This work was supported by National Natural Science Foundation of China (No. 21276087).

References

[1] S. Iijima, Helical microtubules of graphitic carbon, Nature 354 (1991) 56–58.
[2] P. Simon, Y. Gogotsi, Materials for electrochemical capacitors, Nat. Mater. 7 (2008) 845–854.
[3] A.K. Sahu, K.G. Nishanth, G. Selvarani, P. Sridhar, S. Pitchumani, A.K. Shukla, Polymer electrolyte fuel cells employing electrodes with gas-diffusion layers of mesoporous carbon derived from a sol–gel route, Carbon 47 (2009) 102–108.
[4] B. Corry, Designing carbon nanotube membranes for efficient water desalination, J. Phys. Chem. B 112 (2008) 1427–1434.
[5] G.C. Chen, X.Q. Shan, Y.S. Wang, Z.G. Pei, X.E. Shen, B. Wen, Effects of copper, lead, and cadmium on the sorption and desorption of atrazine onto and from carbon nanotubes, Environ. Sci. Technol. 42 (2008) 8297–8302.
[6] M.S. Mauter, M. Elimelech, Environmental applications of carbon-based nanomaterials, Environ. Sci. Technol. 42 (2008) 5843–5859.
[7] W.Z. Li, S.S. Xie, L.X. Qian, B.H. Chang, B.S. Zou, W.Y. Zhou, R.A. Zhao, G. Wang, Large-scale synthesis of aligned carbon nanotubes, Science 274 (1996) 1701–1703.
[8] G.F. Zou, D.W. Zhang, C. Dong, H. Li, K. Xiong, L.F. Fei, Carbon nanofibers: Synthesis, characterization, and electrochemical properties, Carbon 44 (2006) 828–832.
[9] M.K. Lee, A.J. Dillen, J.W. Geus, K.P. Jong, J.H. Bitter, Catalytic growth of macroscopic carbon nanofiber bodies with high bulk density and high mechanical strength, Carbon 44 (2006) 629–637.
[10] J.D. Fowlkes, A.V. Melechko, K.L. Klein, P.D. Rack, D.A. Smith, D.K. Hensley, Control of catalyst particle crystallographic orientation in vertically aligned carbon nanofiber synthesis, Carbon 44 (2006) 1503–1510.
[11] S.S. Fan, M.G. Chapline, N.R. Franklin, T.W. Tombler, A.M. Cassell, H.J. Dai, Self-oriented regular arrays of carbon nanotubes and their field emission properties, Science 283 (1999) 512–514.
[12] D. Park, Y.H. Kim, J.K. Lee, Synthesis of carbon nanotubes on metallic substrates by a sequential combination of PECVD and thermal CVD, Carbon 41 (2003) 1025–1029.
[13] Y.S. Li, A. Hirose, Controlled synthesis of diamond and carbon nanotubes on Ni-base alloy, Appl. Surf. Sci. 255 (2008) 2251–2255.
[14] Y. Gao, L.K. Pan, Y.P. Zhang, Y.W. Chen, Z. Sun, Electrosorption of $FeCl_3$ solutions with carbon nanotubes and nanofibers film electrodes grown on graphite substrates, Surf. Rev. Lett. 14 (2007) 1033–1037.
[15] H.B. Li, Y. Gao, L.K. Pan, Y.P. Zhang, Y.W. Chen, Z. Sun, Electrosorptive desalination by carbon nanotubes and nanofibres electrodes and ion-exchange membranes, Water Res. 20 (2008) 4923–4928.
[16] H.B. Li, L.K. Pan, Y.P. Zhang, L. Zou, C.Q. Sun, Y.K. Zhan, Z. Sun, Kinetics and thermodynamics study for electrosorption of NaCl onto carbon nanotubes and carbon nanofibers electrodes, Chem. Phys. Lett. 485 (2010) 161–166.
[17] X.Z. Wang, M.G. Li, Y.W. Chen, R.M. Cheng, S.M. Huang, L.K. Pan, Z. Sun, Electrosorption of ions from aqueous solutions with carbon nanotubes and nanofibers composite film electrodes, Appl. Phys. Lett. 89 (2006) 053127–1–3.
[18] Q.L. Bao, C.X. Pan, Electric field induced growth of well aligned carbon nanotubes from ethanol flames, Nanotechnology 17 (2006) 1016–1021.
[19] Q.L. Bao, H. Zhang, C.X. Pan, Electric-field-induced microstructural transformation of carbon nanotubes, Appl. Phys. Lett. 89 (2006) 063124–1–3.
[20] E. Fraackowiak, K. Jurewicz, K. Szostak, S. Delpeux, F. Beguin, Nanotubular materials as electrodes for supercapacitors, Fuel. Process. Technol. 77–78 (2002) 213–219.
[21] J.W. Shim, S.J. Park, S.K. Ryu, Effect of modification with HNO_3 and NaOH on metals adsorption by pitch-based activated carbon fiber, Carbon 39 (2001) 1635–1642.
[22] R. Andrews, D. Jacques, D. Qian, E.C. Dickey, Purification and structural annealing of multiwalled carbon nanotubes at graphitization temperatures, Carbon 39 (2001) 1681–1687.
[23] E. Frackowiak, S. Delpeux, K. Jurewicz, K. Szostak, D. Cazorla-Amoros, F. Beguin, Enhanced capacitance of carbon nanotubes through chemical activation, Chem. Phys. Lett. 361 (2001) 36–41.
[24] B.E. Conway, Electrochemical Supercapacitors: Scientific Fundamental and Technological Applications, Plenum Publishers, New York, NY, 1999.
[25] K.L. Yang, T.Y. Ying, S. Yiacoumi, C. Tsouris, E.S. Vittoratos, Electrosorption of ions from aqueous solutions by carbon aerogel: An electrical double-layer model, Langmuir 17 (2001) 1961–1969.